An Electrochemical, Microtopographical and Ambient Pressure X-Ray Photoelectron Spectroscopic Investigation of Si/TiO_2/Ni/Electrolyte Interfaces

Michael F. Lichterman,[a,b,=] Matthias H. Richter,[a,b,=] Shu Hu,[a,b,=] Ethan J. Crumlin,[c,=] Stephanus Axnanda,[c] Marco Favaro,[c,d,e] Walter Drisdell,[d,e] Zahid Hussain,[c] Bruce S. Brunschwig,[b,f] Nathan S. Lewis,[a,b,f,g,*] Zhi Liu,[c,h,i] and Hans-Joachim Lewerenz[b,*,z]

[a]*Division of Chemistry and Chemical Engineering, California Institute of Technology, Pasadena, California 91125, USA*
[b]*Joint Center for Artificial Photosynthesis, California Institute of Technology, Pasadena, California 91125, USA*
[c]*Advanced Light Source, Lawrence Berkeley National Laboratory, Berkeley, California 94720, USA*
[d]*Materials Science Division, Lawrence Berkeley National Laboratory, Berkeley, California 94720, USA*
[e]*Joint Center for Artificial Photosynthesis, Lawrence Berkeley National Laboratory, Berkeley, California 94720, USA*
[f]*Beckman Institute, California Institute of Technology, Pasadena, California 91125, USA*
[g]*Kavli Nanoscience Institute, California Institute of Technology, Pasadena, California 91125, USA.*
[h]*State Key Laboratory of Functional Materials for Informatics, Shanghai Institute of Microsystem and Information Technology, Chinese Academy of Sciences, Shanghai 200050, People's Republic of China*
[i]*School of Physical Science and Technology, ShanghaiTech University, Shanghai 200031, People's Republic of China*

The electrical and spectroscopic properties of the TiO_2/Ni protection layer system, which enables stabilization of otherwise corroding photoanodes, have been investigated in contact with electrolyte solutions by scanning-probe microscopy, electrochemistry and in-situ ambient pressure X-ray photoelectron spectroscopy (AP-XPS). Specifically, the energy-band relations of the p^+-Si/ALD-TiO_2/Ni interface have been determined for a selected range of Ni thicknesses. AP-XPS measurements using tender X-rays were performed in a three-electrode electrochemical arrangement under potentiostatic control to obtain information from the semiconductor near-surface region, the electrochemical double layer (ECDL) and the electrolyte beyond the ECDL. The degree of conductivity depended on the chemical state of the Ni on the TiO_2 surface. At low loadings of Ni, the Ni was present primarily as an oxide layer and the samples were not conductive, although the TiO_2 XPS core levels nonetheless displayed behavior indicative of a metal-electrolyte junction. In contrast, as the Ni thickness increased, the Ni phase was primarily metallic and the electrochemical behavior became highly conductive, with the AP-XPS data indicative of a metal-electrolyte junction. Electrochemical and microtopographical methods have been employed to better define the nature of the TiO_2/Ni electrodes and to contextualize the AP-XPS results.
 [DOI: 10.1149/2.0861602jes]

Manuscript submitted September 9, 2015; revised manuscript received November 16, 2015. Published December 5, 2015.

Photoelectron spectroscopy can be used to directly characterize the energy relations of semiconductor/liquid junctions that underlie the operation of photoelectrochemical cells,[1] provided that the kinetic energy of the emitted photoelectrons can elastically penetrate the water film on the electrode surface. Conventional X-ray photoelectron spectroscopy (XPS) experiments are performed in ultra-high vacuum (UHV) in the absence of electrolyte, and thus do not allow for electrochemical control of an operating device during collection of XPS data. Recent theoretical work has shown that the inclusion of structured solvation layers on electrodes can alter the surface dipole by 0.5–0.7 eV (1.9–2.1 eV) for IrO_2 (WO_3).[2] Established *in-system* techniques that allow analyses of (photo)electrodes after electrochemical operation enable assessment of aspects of the surface chemistry and of the associated energetic behavior.[3–5] However, such experiments are limited in scope and interpretation due to the rinsing, drying and outgassing procedures required prior to insertion of the sample into the UHV analysis chamber. In contrast, the use of tender X-rays having photon energies in the 2.3–5.2 keV energy range allows generation of photoelectrons that have a substantially increased inelastic mean free path. This approach allows "operando" XPS studies in conjunction with a classical three-electrode potentiostatic arrangement and also facilitates investigation of the influence of the applied potential on the band-edge energies of metal, semiconductor and hybrid electrodes at such interfaces.[6,7] Band bending and band-edge shifts can thus be determined directly by this spectroscopic technique.[7]

We describe herein surface-sensitive analysis techniques for the characterization of TiO_2/Ni/electrolyte interfaces. The protection and stabilization of photoanodes for water oxidation to O_2(g) is of interest because high performance and stability can be achieved simultaneously by protecting a variety of otherwise unstable semiconductor photoanodes.[8–11] Specifically, TiO_2 has been used as a protection layer for photoelectrodes in either alkaline or acidic media.[7,12–17] Some work indicates that annealing the TiO_2 allows for charge conduction with minimal band bending, with unannealed TiO_2 preferred for photocathodes. However, the role of the metallization layer in determining the charge-conduction properties of the films has not been well elucidated.[18] A thin layer of TiO_2 can protect Si and allows for water oxidation with an Ir oxygen-evolution catalyst, but in such systems increasing the thickness of the TiO_2 film beyond 2 nm led to a substantial increase in resistance, such that a 10 nm film was nearly nonconductive even when contacted with Ir.[11] In contrast, TiO_2 has been found to be a nearly ideal protection layer from the viewpoint of the band-edge alignment when used on p-InP or p-Si photocathodes.[19,20] Thus, while the band positions of the TiO_2 films appear to be inherently conducive to photocathode protection, the nature of the TiO_2/(metal)/electrolyte contact requires further investigation. Specifically, when contacted with Ni metal, TiO_2 films allow for the sustained use of highly efficient semiconductor materials (Si, III-V, II-VI) for water splitting and in other oxidizing environments, especially in alkaline media where efficient, intrinsically safe solar-driven water-splitting systems can be built.[12,13]

We describe herein the use of a three-electrode photoelectrochemical cell that contains a meniscus-based ~13 nm thick electrolyte on the working electrodes formed from p^+-Si/TiO_2/Ni interfaces, which allows XPS measurements under electrochemical control through the solution.[6,7] Combined electrochemistry-photoelectron spectroscopic data that extend the previous characterization of this system[7] have been collected in this work.

Degenerately doped Si was used as a back contact for the TiO_2 to ensure that the changes in the observed binding energies originated from electric fields (or their absence) in the TiO_2 and not in the underlying Si. (Photo)electrochemical and microtopographical char-

[=]These authors contributed equally to this work.
*Electrochemical Society Active Member.
[z]E-mail: lewerenz@caltech.edu

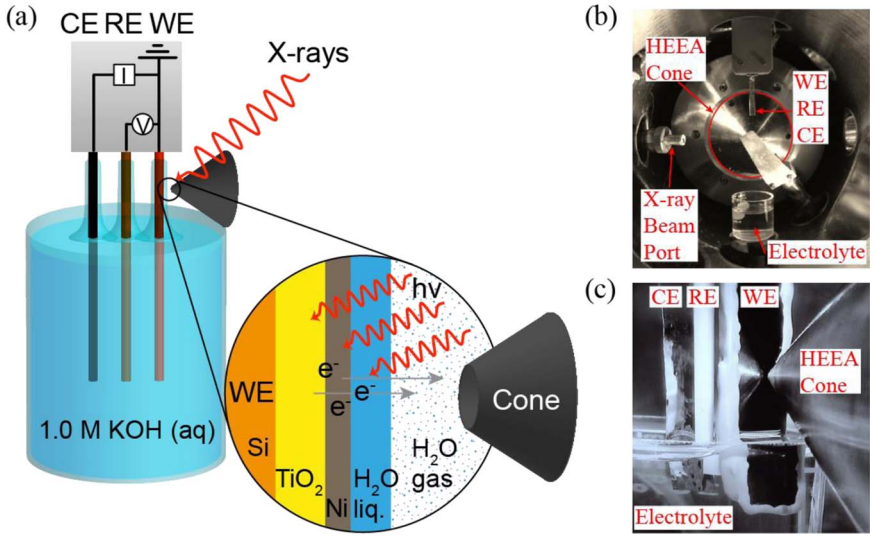

Figure 1. (a) Scheme of the *operando* XPS-PEC setup. The working electrode and the hemispherical electron energy analyzer (HEEA) were grounded to each other. The potential of the working electrode was changed with respect to the reference electrode. The PEC-beaker containing the electrolyte could be moved in the z direction whereas the three-electrode mount could be moved in the x-, y-, and z-directions. (b) View into the high-pressure analysis chamber. The X-ray beam enters through the window on the left, the three-electrode setup is on the top, the electrolyte beaker on the bottom, and the electron analyzer cone is in the center. (c) Three-electrode setup pulled up and in measurement position (compare to (a)).

acterization using scanning probe microscopy have additionally been performed to assess the nature of the electrode surfaces and their conductivity properties as a function of the amount of metal deposited onto the TiO_2-coated photoanode surface. Recent work[15] in addition to work from our labs[7,12,13,17] suggests that the presence or absence of band bending is a key factor for facilitating charge conduction through these films. The experiments reported herein demonstrate that the degree of band-bending in a semiconductor (photo)electrode is not the only parameter that allows for charge conduction. The data also indicate that metallization that decreases the band bending is necessary for conduction. Hence multiple parameters must be optimized to obtain a functional protected photoelectrode.

Experimental

Films of TiO_2 were produced by atomic-layer deposition (ALD)[12,13,21,22] on degenerately doped p-type silicon ("p^+-Si") substrates. (100)-oriented boron doped Si wafers with a resistivity $\rho <$ 0.005 Ω·cm were first cleaned *via* an oxidizing etch, with the Si soaked for 2 min in a 3:1 (by volume) "piranha" solution of concentrated H_2SO_4 (98%) to 30% H_2O_2(aq), followed by an etch for 10 s in a 10% (by volume) solution of HF(aq). The wafers were then immediately etched in a 5:1:1 (by volume) solution of H_2O, 36% hydrochloric acid, and 30% hydrogen peroxide for 10 min at 75 °C before being moved into the ALD chamber. The TiO_2 was deposited from a tetrakis(dimethylamido)titanium (TDMAT) precursor in a Cambridge Nanotech Savannah ALD reactor. In an ALD cycle, a 0.1 s pulse of TDMAT was followed by a 15 s purge of N_2 at 20 sccm, followed by a 0.015 s pulse of H_2O before another 15 s purge with N_2. This process was repeated for 1500 cycles to provide films ∼70 nm in thickness. Where desired, Ni was deposited at a rate of ∼2 nm per min by use of a RF sputtering power of 150 W for 20 s–300 s in an AJA-International sputtering system. The time used to sputter the Ni is denoted herein as t_{sp}.

Atomic-force microscopy (AFM) data were collected using a Bruker Dimension Icon AFM, using Peakforce Quantitative Nanomechanical parameters, to provide information on the height, adhesion and deformation of the sample surface. ScanAsyst mode was used to optimize the tapping frequency and other experimental parameters, e.g. the gain, set point, and cantilever tuning. ScanAsyst-Air tips (silicon nitride) were used, with a nominal tip radius of 2 nm and a rotated (symmetric) geometry.

Electrochemical characterization was performed at a scan rate of 50 mV s^{-1} in either 1.0 M KOH(aq) or 50/350 mM $Fe(CN)_6^{3-/4-}$(aq), using Biologic SP-200 and SP-300 potentiostats. In KOH, a leak-free Ag/AgCl reference electrode (eDAQ) and a platinum counter electrode were used. For measurements in $Fe(CN)_6^{3-/4-}$(aq), the reference and counter electrodes were each Pt mesh electrodes.

Operando AP-XPS experiments were performed at the Advanced Light Source, Berkeley at the tender X-ray beamline 9.3.1.[6,7] Fig. 1 presents schematically the geometry of the end station. Potentials were applied between the reference electrode, E_{REF}, and the Fermi energy, E_F, of the working electrode. X-rays at an energy of 4 keV were selected from a range of 2.3 keV–5.2 keV with an energy resolution of $E/\Delta E$ = 3000–7200. The X-ray beam spot size at the beam line was 1 mm x 2 mm.[6] The photoelectron collection cone was aligned to the beam line X-ray spot at a distance of ∼300 μm (Fig. 1). The experiments were performed using an electrochemical cell with a hanging meniscus "emersion" configuration. Negligible steady-state faradaic current was passed at the potentials used in the experiments described herein. We designate this condition as "*operando*" because the observed region of the working electrode was under potential control and the working electrode itself comprised an isopotential surface. The pressure in the sample chamber was between 20 and 27 mbar, which is considered ambient pressure in the context of X-ray spectroscopy. To prepare electrodes for *operando* AP-XPS, strips of the p^+-Si/TiO_2/(Ni) wafers were cut into 1 cm × 3.5 cm rectangles. Highly doped p^+-Si was used simultaneously as a support material as well as to provide an effective back contact to the ALD-TiO_2. The ohmic contact at the back of the semiconductor was connected to the photoelectron analyzer to provide a high conductivity ground for the sample. To make ohmic contact to the sample, an In/Ga eutectic was scribed into the back of the Si wafer, and Ag paint was used to contact the electrode to a strip of Cu tape that was supported on a 0.8 cm × 3 cm glass slide.

Results

TiO_2/Ni/electrolyte structures having varying thicknesses of Ni were analyzed in detail. The Ni thickness is referred to by the sputter deposition time, t_{sp}, as described in the Experimental section. For short deposition times, the Ni films were incomplete and non-uniform. Thus, the deposition time is more informative than a calculated thickness, and hence t_{sp} has been quoted herein as the independent variable that was varied experimentally to produce the different interfaces under study.

Electrochemical characterization.— Deposition of Ni onto relatively thick (44 nm to 150 nm) ALD-grown TiO_2 enables charge conduction through the TiO_2.[12,13] In previous photoelectrochemical analyses,[12,13] Ni deposits consisted either of large islands (3 × 7 micron grid) or of thin, t_{sp} ∼120 s, sputtered Ni films. Herein we

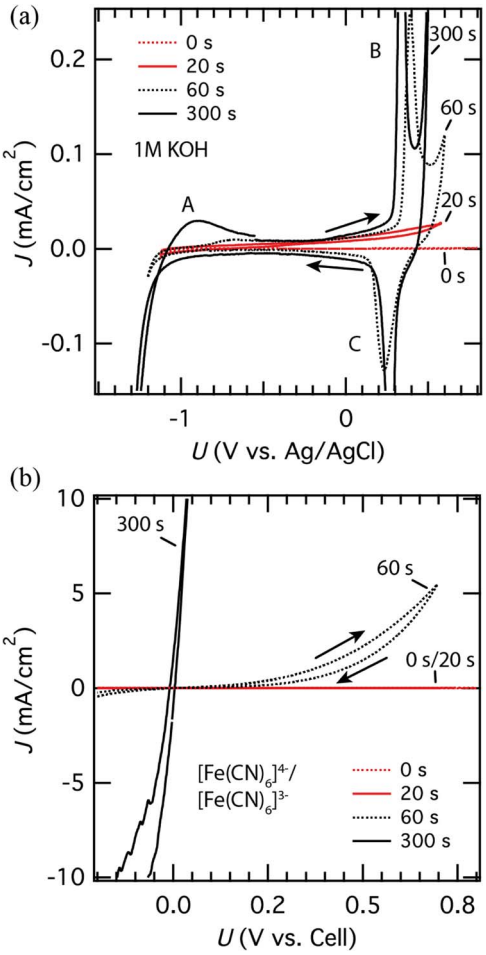

Figure 2. (a) *J-U* data collected for bare TiO_2, TiO_2/Ni (20 s), TiO_2/Ni (60 s), and TiO_2/Ni (300 s) electrodes, respectively, in 1.0 M KOH(aq). Three peaks were observed: for $t_{sp} = 60$ s, an anodic peak A at −0.7 V, an anodic peak B at +0.39 V, and a cathodic peak at +0.23 V vs. Ag/AgCl. For $t_{sp} = 300$ s, these peaks shifted to −0.85 V, +0.34 V and +0.28 V vs. Ag/AgCl. (b) *J-U* data measured in 50/350 mM $Fe(CN)_6^{3-/4-}$(aq) solution. Arrows show the scan direction.

investigate the characteristics of interfaces formed by deposition of a variety of Ni layer thicknesses.

Fig. 2a shows the current density vs. potential (*J-U)* characteristics of TiO_2/Ni electrodes in 1.0 M KOH formed using Ni deposition times of 0 s, 20 s, 60 s, or 300 s. The *J-U* sweeps were initiated in the positive direction from the open-circuit potential, U_{OC}. The data were recorded after completion of the AP-XPS measurements, to establish the interrelation of the voltammograms with the photoelectron spectra. Five main features were observed in the voltammetric data for TiO_2/Ni (60 s) and TiO_2/Ni (300 s) interfaces. For $t_{sp} = 60$ s, the onset of hydrogen evolution (HER) occurred at −1.1 V vs. Ag/AgCl, and an anodic peak, wave A, was observed at $U = -0.7$ V vs. Ag/AgCl, attributable to the oxidation of metallic Ni(0) to Ni(II).[23] The related cathodic peak associated with the reduction of Ni(II) to Ni(0) was not observed. At positive potentials, the *J-U* data exhibited an oxidative transformation at $U = +0.39$ V (wave B; anodic current) ascribable to Ni(II) to Ni(III), prior to the onset of the oxygen-evolution reaction (OER) at +0.52 V vs. Ag/AgCl. A reductive peak at $U = +0.23$ V vs. Ag/AgCl (wave C; cathodic current) was observed on the return sweep. For $t_{sp} = 300$ s, the anodic and cathodic waves at +0.34 V and +0.28 V vs. Ag/AgCl, respectively, exhibited less separation, and the catalytic OER current was observed at 0.49 V vs. Ag/AgCl. The samples that had lower catalyst loadings, e.g. $t_{sp} = 20$ s, did not display the Ni(0)/Ni(II) and Ni(II)/Ni(III) redox peaks.

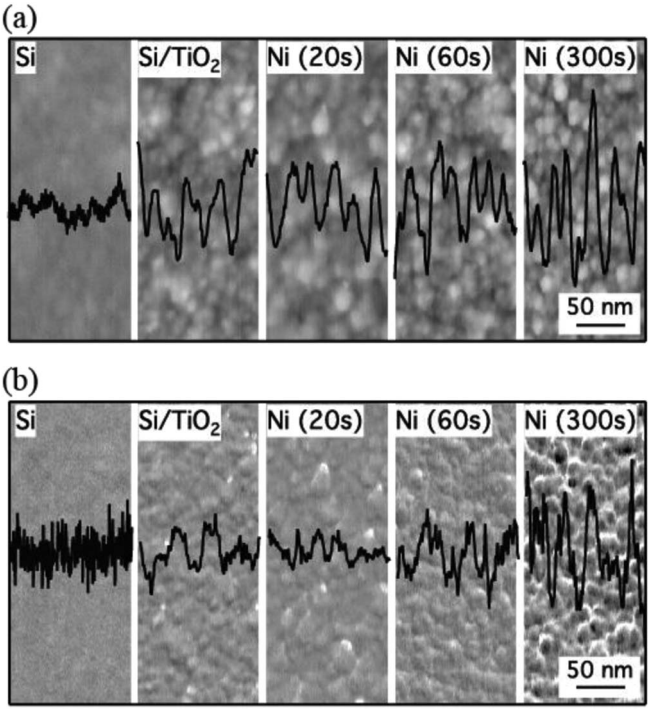

Figure 3. AFM microtopographs of bare silicon, ~70 nm thick TiO_2 on silicon, Si/TiO_2/Ni (20 s), Si/TiO_2/Ni (60 s), and Si/TiO_2/Ni (300 s). (a) depicts the height information and (b) the surface deformation by the AFM tip. The sub-micrographs in (a) and (b) have the same height scaling. In each graph the insets show line scans from the middle of the microtopographs.

Fig. 2b shows the electrochemical data obtained when the electrodes were in contact with $Fe(CN)_6^{3-/4-}$(aq). An analogous trend was observed, and only electrodes with Ni thicknesses of >2 nm (sputter times ≥ 60s) exhibited substantial current flow, even in the presence of an electrochemically reversible one-electron redox couple.

Surface Microtopography.— Tapping mode AFM data were obtained to determine the coverage and structure of the Ni overlayer (Fig. 3). Only minor differences (~4%) in roughness between bare TiO_2 and TiO_2 with $t_{sp} = 20$ s or 60 s of Ni deposition (Table I) were observed in the sample height data obtained using peak force quantitative nanomechanical measurements (Fig. 3a). However, a local minimum in deformation was observed for the electrode that had been coated with Ni for 20 s. For increased sputter times, i.e. for the sample with $t_s = 300$ s, much higher roughness (~30%) and deformations (~160%) were observed. Electrodes having $t_{sp} = 60$ s generally were very similar to the behavior observed for bare TiO_2.

Table I. Surface roughness parameters obtained by AFM for the height distribution and the surface deformation. While the surface roughness and deformation parameters stay nearly constant up to 60 s (with a minimum for 20 s) the change (increase by up to 160%) of the surface properties is more drastic after Ni deposition with a 300 s sputter time.

	Height		Deformation	
Ni\Roughness	RMS (nm)	Ra (nm)	RMS (nm)	Ra (nm)
0 sec	0.71	0.55	0.17	0.12
20 sec	0.68	0.53	0.14	0.10
60 sec	0.69	0.55	0.17	0.13
300 sec	0.91	0.72	0.44	0.33

Junction energy relations: AP-XPS.— TiO_2/(Ni) electrodes were examined by AP-XPS in a manner analogous to that described previously,[7] with Ni deposited for t_{sp} = 0 s, 20 s, 60 s, or 300 s, respectively. The binding energy, E_B, of a core level can be calculated as $E_B = h\nu - E_{K,VAC} - \phi_{sample}$ where $E_{K,VAC}$ is the kinetic energy of the photoelectron with respect to the vacuum energy level (E_{VAC}), ϕ_{sample} is the work function of the sample, and $h\nu$ is the X-ray energy. E_B is measured relative to the Fermi energy, E_F, of the analyzer (or of the sample, which are equal, because the two components are in electrical contact). However ϕ_{sample} is unknown during the XPS measurements, and the kinetic energy is referenced to the Fermi energy, E_F, if not otherwise noted, i.e. $E_K = E_{K,VAC} + \phi_{sample}$ (where ϕ_{sample} is the energetic difference between E_{VAC} and the Fermi level of the sample). This approach provides binding energies that are referenced to the analyzer. To provide a description from an electrochemical perspective, we define E_B' as the core-level binding energy referenced to the solution potential instead of being referenced to E_F of the working electrode/analyzer. Because the potentials are set at the working electrode with respect to the reference electrode, E_B' can be defined by Eq. 1

$$E_B' = E_B + qU_{eff} \quad [1]$$

where q is the absolute charge of an electron and U_{eff} tracks the difference in the electrochemical potentials between the solution and the working electrode. U_{eff} is given by $U_{eff} = U - U_{FB}$ where U is the applied potential and U_{FB} is the flatband potential for the bare TiO_2 electrode (for details see Ref. 7). Hence the solution-corrected core-level binding energy, E_B', measures the binding energy of a level relative to the solution potential. In this approach, the solution-corrected binding energies E_B' of core levels of materials in solution, such as the O 1s level of solution (bulk) water, should remain constant as the potential at the working electrode is varied (the effect of water in the double layer is negligible at the ionic strengths used). Semiconductors that have "fixed" band edges in a semiconductor/liquid junction should show no change in E_B' at the interface with a change in U_{eff}, because in this picture, the band edges are fixed relative to the solution energetics. However, for cases in which the band edges of the semiconductor shift, such as in the case of accumulation or Fermi-level pinning due to defect states,[7] the solution-corrected binding energy would be expected to shift with respect to the solution potential. Thus when the binding energy is referenced to the solution potential or to the potential of the reference electrode, the E_B' of the water O 1s level and of the semiconductor/liquid junction semiconductor core levels would be expected to be independent of the solution potential, and should exhibit a shift parameter $\Delta' \equiv \partial E_B'/\partial U_{eff} = 0$ eV V^{-1}. However, for cases where the band edges shift with respect to the solution, as may result from Fermi level pinning, a change in the solution-corrected binding energies with solution potential is expected. This situation can be contrasted with the results expected when the binding energies are determined with respect to the analyzer,[7] because when referencing binding energies to the analyzer (E_B), the water O 1s and pure (without metallization) semiconductor/liquid junction semiconductor core levels are expected to show a shift $\Delta \equiv \partial E_B/\partial U_{eff} = \Delta = -1$ eV V^{-1} with respect to the applied voltage.[7]

Fig. 4 plots solution-corrected XPS spectra for the O 1s and Ti 2p core levels for a bare TiO_2 electrode, in which the photoemission intensities are plotted against E_B', and Fig. 5 plots the solution-corrected XPS spectra for the Ni 2p, O 1s and Ti 2p core levels of the TiO_2/Ni (20 s) electrode vs E_B'. The bare TiO_2 XPS peaks showed less band-edge shifting whereas electrodes with Ni showed a larger shift. Fig. 6a displays the full width at half maximum (FWHM) of the liquid water O 1s core level, as well as of the TiO_2 O 1s peak, for the bare TiO_2 electrode. The FWHM data are expected to reach a minimum at the flatband potential.[7] Fig. 6a shows that for the bare TiO_2 electrode, the FWHM for the TiO_2 O 1s peak reaches a minimum at −0.9 V vs. Ag/AgCl. Fig. 6b shows the solution-corrected core level shift for the Ti $2p_{3/2}$ core levels across a range of potentials for the three different TiO_2/(Ni) electrodes. The slopes, Δ'_{Ti}, of the fitted lines show that the solution-referenced binding energy E_B' of the Ti $2p_{3/2}$ core level shifted with a slope of 1.0 ± 0.08 eV V^{-1} for TiO_2/Ni (20 s), 0.9 ± 0.10 eV V^{-1} for TiO_2/Ni (60 s), and 1.0 ± 0.07 eV V^{-1} for TiO_2/Ni (300 s). Fig. 6c shows that the relative peak shift, Δ'_{Ni}, of E_B' for the Ni $2p_{3/2}$ core level for TiO_2/Ni (20 s) was 0.7 ± 0.07 eV V^{-1}; that for TiO_2/Ni (60 s) was 0.9 ± 0.08 eV V^{-1}; and the value for TiO_2/Ni (300 s) was 1.0 ± 0.08 eV V^{-1}. The errors associated with these slopes result primarily from the resolution of, and uncertainty inherent to, the measurement.

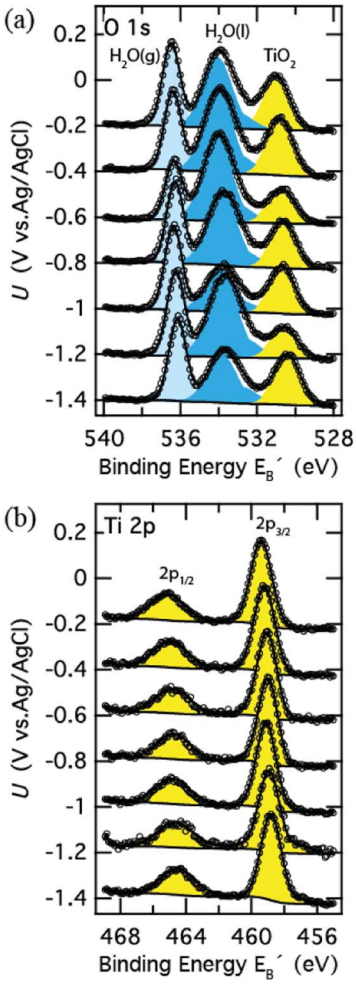

Figure 4. O 1s (a) and Ti 2p (b) X-ray photoemission spectra of the bare TiO_2 electrode in 1.0 M KOH(aq) for $U = -1.4$ V to −0.2 V vs. Ag/AgCl. The binding energies are referenced to the solution potential as explained in the text and corrected by the applied potential with respect to flatband conditions at $U_{FB} = -0.9$ V vs. Ag/AgCl.[7]

Fig. 7 displays XPS data showing the Ni $2p_{3/2}$ core level for samples prepared with t_{sp} = 20 s, 60 s and 300 s. The electrode was maintained at a potential of −1.0 V vs. Ag/AgCl, and the Ni(0), Ni(II), and Ni(III) peaks as well as the satellite peaks are labeled. A clear lack of a metallic Ni phase was observed for the t_{sp} = 20 s sample at potentials positive of flatband, and only a very small amount of metallic Ni (6%, Ni $2p_{3/2}$ peak area) was visible under reducing conditions at $U = -1.0$ V vs. Ag/AgCl. In contrast, the t_{sp} = 60 s sample had a significant peak area fraction (40%) of metallic Ni and the sample prepared using t_{sp} = 60 s showed a large fraction (51%) of metallic Ni. The Ni(III) content was 94% for t_{sp} = 20 s, 47% for t_{sp} = 60 s and 22% for t_{sp} = 300 s, based on peak areas in the Ni $2p_{3/2}$ peak.

Discussion

Electrochemistry.— For lower Ni coverage, the electrode exhibited resistive behavior with very low currents in both the KOH electrolyte

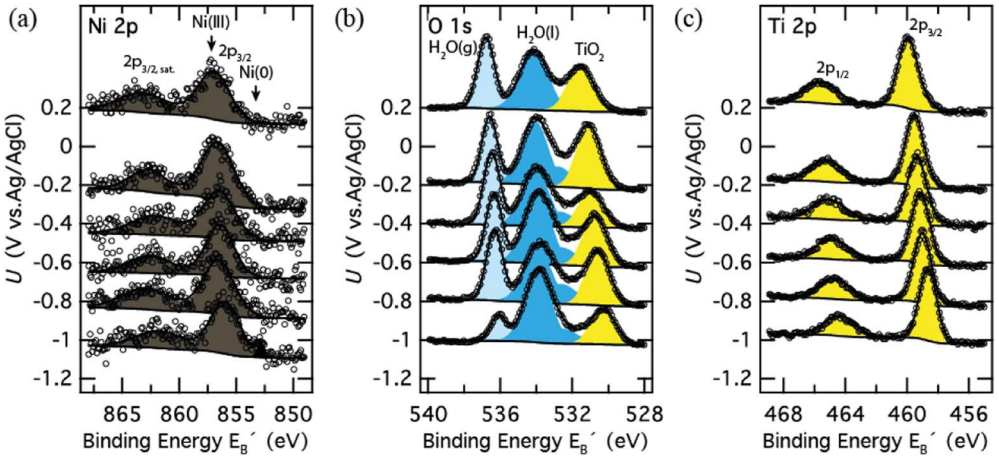

Figure 5. Ni 2p (a), O 1s (b), and Ti 2p (c) X-ray photoemission spectra of a TiO_2/Ni (20 s) electrode in 1.0 M KOH(aq) for $U = -1.0$ V to $+0.2$ V vs. Ag/AgCl. The binding energies are referenced to the solution potential as explained in the text and corrected by the applied potential with respect to flatband conditions at $U_{FB} = -0.9$ V vs. Ag/AgCl[7] (see Eqs. 1 and 2). The positions of metallic (Ni(0)) and fully oxidized Ni (Ni(III)) are indicated in (a) by arrows.

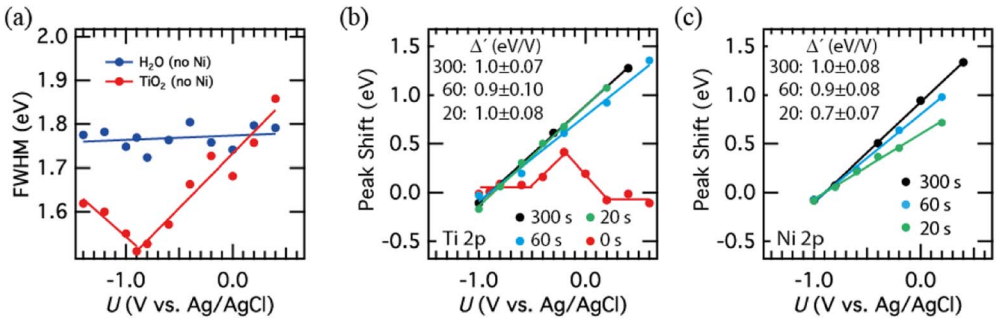

Figure 6. (a) Full width at half maximum (FWHM) peak data for the water O 1s and TiO_2 O 1s core levels for a bare TiO_2 electrode. (b) The core level peak shifts with respect to the binding energy at flatband, which indicate the band-edge shift of the semiconductor with respect to the electrolyte, of the Ti $2p_{3/2}$ core level for TiO_2/electrolyte, TiO_2/Ni (20 s)/electrolyte, TiO_2/Ni (60 s)/electrolyte, and TiO_2/Ni (300 s)/electrolyte geometries. (c) Similar to (b) but plotting only the Ni $2p_{3/2}$ core level peak shift for the $t_{sp} = 20$ s, 60 s, and 300 s electrodes. The binding energies are referenced to the solution potential as explained in the text, and are corrected by the applied potential with respect to flatband conditions at $U_{FB} = -0.9$ V vs. Ag/AgCl[7] (see Eqs. 1 and 2).

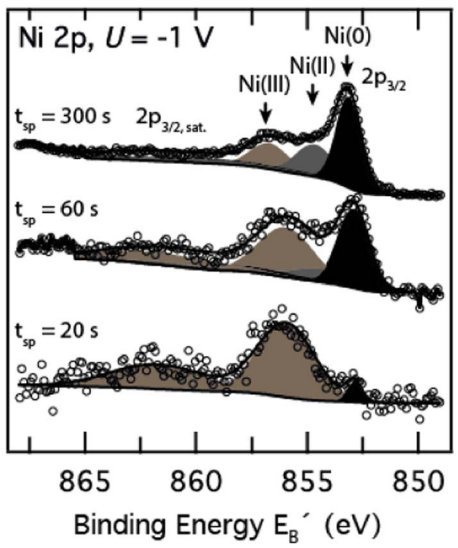

Figure 7. Ni $2p_{3/2}$ X-ray photoemission spectra for $t_{sp} = 20$ s, 60 s, and 300 s for $U = -1$ V vs. Ag/AgCl. The binding energies are referenced to the solution potential as explained in the text and corrected by the applied potential with respect to flatband conditions at $U_{FB} = -0.9$ V vs. Ag/AgCl[7] (see Eqs. 1 and 2). The positions of metallic (Ni(0)), Ni(II), and fully oxidized Ni (Ni(III)) are indicated by arrows.

and the $Fe(CN)_6^{3-/4-}$ redox solution (Fig. 2). However, currents became substantial for the electrode that had $t_{sp} = 60$ s (~2 nm) of Ni. The typical electrochemical signatures of Ni oxidation and reduction as well as HER and OER were observed, with the Ni(II)/(III) redox reaction showing irreversible behavior with a peak separation of 0.16 V. Increasing t_{sp} to 300 s decreased this peak separation to 0.06 V, indicating that the conductivity of the sample improved. Starting at the open-circuit potential and scanning toward more positive potentials, the electrodes became covered with NiO, and then NiOOH, as evidenced by the observation of a partial reduction of Ni(III) to Ni(II) (peak C, Fig. 2) in the cathodic branch of the voltammetry. After several cycles in which the potential scan was stopped in the anodic waves, the initially existing Ni metal had been partially oxidized. The corresponding current for Ni oxidation was small because the successfully oxidized Ni overlayers inhibited further oxidation of Ni metal. Prior XPS data on these 2 nm thick Ni films[7] support this conclusion by showing a decrease in the Ni(0) signal with a concomitant increase in the Ni(II) signal. The increase in sample conductivity for thicker Ni coverages is evident in Fig. 2b, where current densities >10 mA cm^{-2} are evident at $+0.1$ V vs. Ag/AgCl. Thus, the data show a distinct difference in the sample conductivity depending on the amount of Ni deposited and on the anodization procedure.[12]

AFM microtopography.— Microtopography data indicated that for small t_{sp} values, the sample exhibited surface roughness and a deformation of the bare TiO_2/solution interface. The dip in the deformation

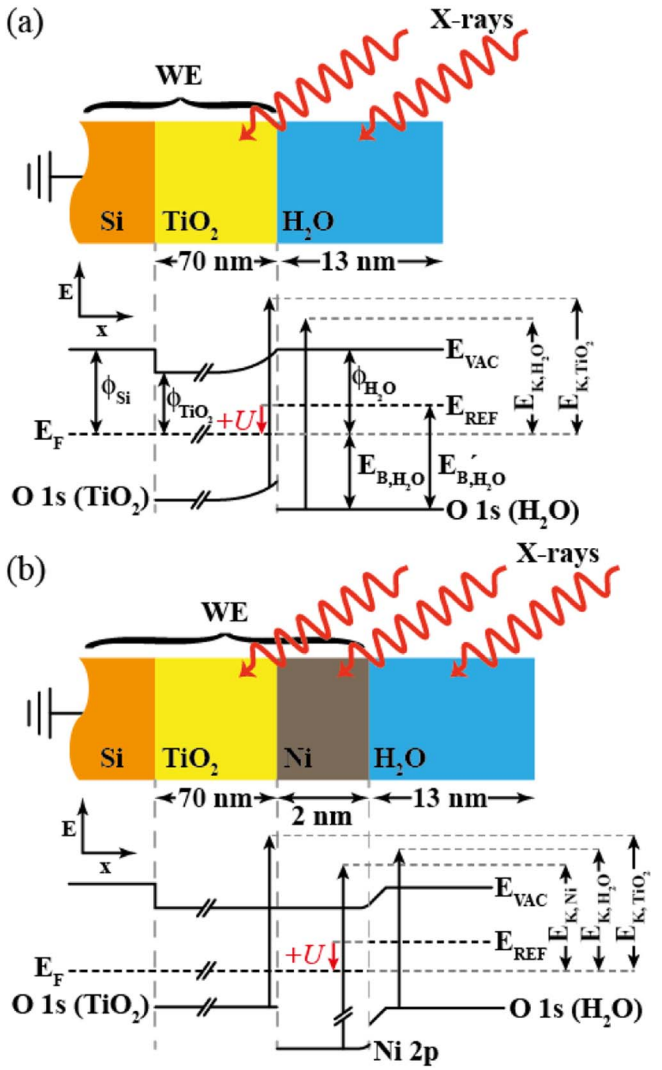

Figure 8. Scheme of the energy-band relations of *operando* photoelectron spectroscopy for (a) the Si/TiO_2/electrolyte geometry and (b) the Si/TiO_2/Ni/electrolyte geometry. The working electrode and analyzer are grounded. A potential is applied to the working electrode in the electrolyte with respect to the reference electrode in a three-electrode configuration. The work function of the material Φ is the difference between the Fermi energy, E_F, and the vacuum energy E_{VAC}. The kinetic energies, $E_K = E_{K,VAC} + \Phi$, of the photoelectrons are measured with respect to the Fermi energy of the analyzer. The binding energy, E_B, is calculated based the photon energy with $E_B = h\nu - E_K = h\nu - E_{K,VAC} - \Phi$ whereas the binding energy with respect to the reference electrode is $E_B' = E_B + qU_{eff}$ (Eq. 1) as illustrated for the binding energy of the water O 1s core level in (a).

data for the t_{sp} = 20 s sample suggests the presence of a different surface material than that observed for either bare TiO_2 or for the thicker Ni-coated TiO_2 surfaces. This behavior is consistent with expectations for a NiO_x/TiO_2 surface that does not contain underlying metallic Ni. The increasing trend in deformation from t_{sp} = 20 s to t_{sp} = 300 s suggests that only after a 20 s deposition of Ni did a substantial metallic phase exist at the TiO_2/NiO_x interface. This conclusion is also supported by XPS data of the Ni 2p core level (Fig. 7).

Energy relations by AP-XPS measurements.— The XPS technique integrates the signal over the spot examined in the experiment. Fig. 8 shows a schematic of the energy-band relations and the resulting description of the structures considered herein. In the physical representation, the kinetic energies plus the work function, E_K, of the photoelectrons are referred to the Fermi level E_F of the working electrode, which coincides with that of the analyzer, to deduce E_B. In the electrochemical frame of reference, kinetic energies are referred to the reference electrode potential to define E_B'. To be consistent, changes in E_B' were measured with respect to the potential at which the flatband condition was observed for the bare TiO_2 electrode. This approach allows evaluation of the shift in the band edges with respect to the solution potential as the applied potential is varied. If the shift in E_B' with potential is greater than zero (see Eq. 1), band-edge movement occurs. Provided that the sampling depth of the technique is smaller than the width of the space-charge region, the shift of E_B, Δ, and of E_B', Δ′, with potential should approximately be related by Eq. 2:

$$\Delta' = \Delta + 1\ \text{eV V}^{-1} \quad [2]$$

Hence, the semiconductor core levels in an ideal semiconductor/liquid junction will have corrected peak shifts Δ′, relative to the reference electrode, of $\Delta' = 0.0\ \text{eV V}^{-1}$; the electrolyte will also exhibit no shift; while the metal core levels in a pure metal/electrolyte junction will shift with the full applied potential *relative to the reference electrode*, i.e. $\Delta' = 1.0\ \text{eV V}^{-1}$.

Analysis of the electrochemical data alone does not directly allow assessment of whether a rectifying or an ohmic contact was formed, because the high resistivity (t_{sp} = 20 s) could also be observed for an isolated system that contains a buried Schottky barrier. The AP-XPS data, however, enables this evaluation of the electrical properties of the materials in the device and at the interfaces of interest.

As shown in Fig. 6b, the average solution-corrected binding energies of the Ti $2p_{3/2}$ core level for the TiO_2/Ni (20 s) interface shifted by 1.0 eV V^{-1}; those for TiO_2/Ni (60 s) shifted by 0.9 eV V^{-1}; and those for TiO_2/Ni (300 s) shifted by 1.0 eV V^{-1}, all showing metal-like behavior. For comparison, the band edges for bare TiO_2 were observed to shift only in the potential range in which defect states occurred, and were otherwise stationary (at potentials more positive than the conduction-band edge)),[7] suggesting that the bare TiO_2 acts like a semiconductor outside of the potential range where the defect states induce Fermi level pinning. Hence, the TiO_2/Ni (20 s), TiO_2/Ni (60 s) and the TiO_2/Ni (300 s) electrodes all exhibited only small amounts of rectification in the underlying TiO_2 layer. The improvements in observed conductivity (Fig. 2) of the TiO_2/Ni electrodes in the order t_{sp} = 0 s < 20 s < 60 s < 300 s therefore likely result from more than simply the removal of rectification in the underlying TiO_2. Furthermore, as shown in Fig. 7, the amount of interfacial metallic Ni increased significantly, with almost no Ni(0) present for t_{sp} = 20 s and half of the layer consisting of Ni(0) for t_{sp} = 300 s. Hence, the data are consistent with the presence of Ni, as opposed to NiO_x, at the TiO_2/Ni interface playing a dominant role in determining the charge conduction through the device.

The importance of the Ni contact, as opposed to NiO_x, to the TiO_2, is evident based on the combination of the electrochemistry (Fig. 2), the solution corrected Ti 2p and Ni 2p core level shifts from AP-XPS data (Fig. 6), and the catalyst compositions (chemical states) from the Ni $2p_{3/2}$ core level AP-XPS (Fig. 7). The bare TiO_2 sample is both nonconductive and observed to be generally rectifying (Figs. 2 and 6), whereas the TiO_2 samples with substantial amounts of metallic Ni ($t_{sp} \geq$ 60 s) are ohmic at the semiconductor/liquid junction (i.e band-edge shifts of $\Delta' \sim 1.0\ \text{eV V}^{-1}$), and are electrically conductive, as evidenced by the *J-U* behavior. The sample with the NiO_x layer (t_{sp} = 20 s) is, therefore, unique, in that it displays similar AP-XPS data in that the band edges of the TiO_2 appear to be similarly disconnected from the solution, such that they shift with respect to the solution potential, as is the case for the samples that have substantial metallic Ni. However, the TiO_2 in the NiO_x-containing samples is nonconductive, as observed in electrochemical analysis (Fig. 2). The junction between NiO_x and TiO_2 appears electronically distinct from that between Ni and TiO_2 in that charge conduction is not present for the NiO_x/TiO_2 structure even though rectification at the TiO_2/liquid junction has largely been removed. If a purely conduction-band transport mechanism operates in the TiO_2, such that Ni metal is not required

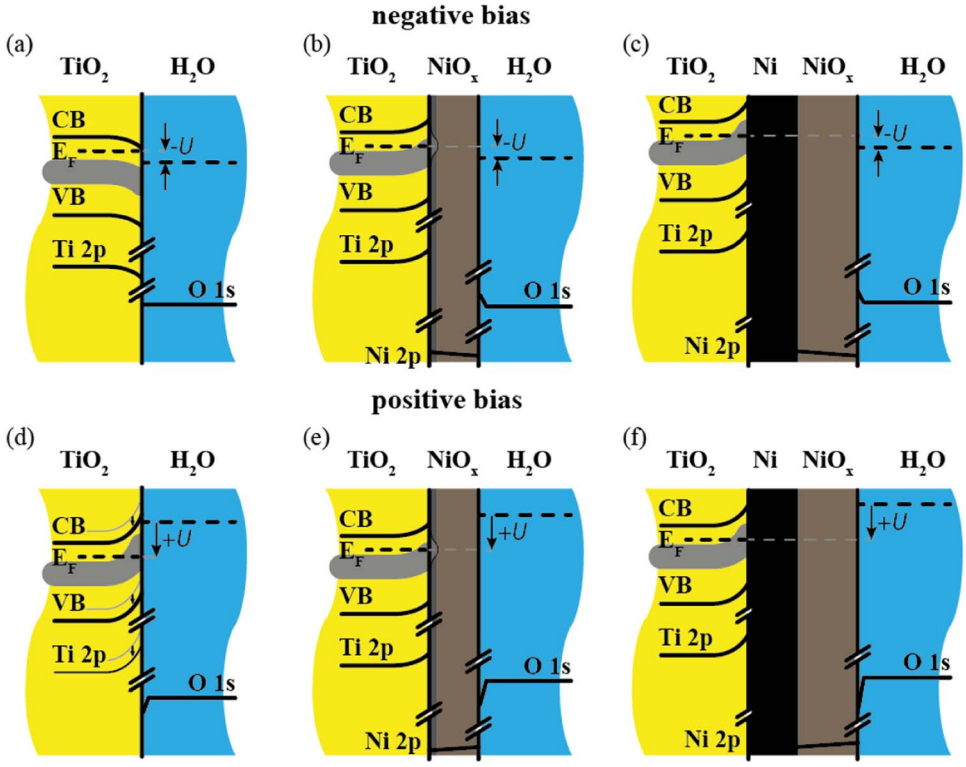

Figure 9. Band diagrams that summarize the experimental findings described herein. (a-c) for negative potential *U* with respect to flatband and (d-f) for positive potential *U* with respect to flatband. The thick gray line marks the position of the mid-gap state band in TiO_2. For (b, c and e, f), Fermi level pinning at the mid-gap states occurs. (a, d) In the absence of Ni or NiO_x, TiO_2 develops a space-charge region with fixed band-edge positions outside of regions involving Fermi-level pinning or accumulation.[7] For increasingly positive potentials, the Fermi level crosses the mid-gap states and band edge shifting in TiO_2 is observed (indicated by the arrows). The potential drop (the amount necessary to charge/discharge the surface states) occurs now in the electrochemical double layer. (b, e) The Fermi energy at the TiO_2/NiO_x interface is pinned near the mid-gap states due to NiO_x interface states. With Fermi level pinning, the band edges shift with the applied potential. (c, f) With a sufficiently dense and thick Ni film at the interface to TiO_2, the TiO_2 band edges are effectively disconnected from the solution, and the presence of metallic Ni allows for charge conduction.

to contact the TiO_2, the loss of rectification for the $t_{sp} = 20$ s sample should have allowed for conduction to be observed for the device in contact with the $Fe(CN)_6^{3-/4-}$ redox solution. Therefore, the lack of conduction in the samples for $t_{sp} = 20$ s is consistent with the presence of NiO_x, as opposed to Ni, heavily influencing the electrical behavior of the TiO_2, leading to an increase in resistivity and a consequent loss in film conductivity. The E_B for the Ti $2p_{3/2}$ core level in the TiO_2/Ni samples with thick Ni was observed to be equal to that observed for the bare TiO_2 films at a potential at the midpoint of the mid-gap states (459.0 eV to 459.1 eV), suggesting an interplay between the mid-gap "defect" states and the Ni overlayer. These results are summarized in Fig. 9 by the schematic energy diagrams of the solid/liquid interface. Figs. 9a–9c shows the situation for negative potentials *U* with respect to the flatband condition, and Figs. 9d–9f depicts the situation for positive potentials *U* with respect to flatband of the TiO_2/electrolyte (Figs. 9a and 9d), TiO_2/NiO_x/electrolyte (Figs. 9b and 9e) and TiO_2/Ni/NiO_x/electrolyte (Figs. 9c and 9f) systems. In the presence of NiO_x and Ni, Fermi level pinning at the mid-gap states occurs. In the absence of Ni or NiO_x, TiO_2 develops a space-charge region with fixed band-edge positions outside of regions involving Fermi-level pinning or accumulation.[7]

Conclusions

The results presented herein demonstrate that *operando* AP-XPS can be used to observe and quantify the degree to which catalysts influence the band energetics of underlying protection layers and the ECDL. In addition to providing information regarding the band energetics, layer composition and chemical state, AP-XPS also provides direct evidence regarding the nature of the rectification and contact at the interface. For various thicknesses of deposited Ni or NiO_x, the rectification in the underlying TiO_2 is mostly removed; however, the increase in conductivity for deposited Ni only occurs when the Ni phase contains a substantial amount of metallic Ni and not merely an oxide phase. As a result, the data indicate that the band lineups between the semiconductor and the metal or metal oxide overlayer, as well as electronic effects that result from this equilibration, are the crucial factors that induce conduction in the TiO_2 films under evaluation. Sufficiently dense metallization allows for stable conduction through such films.

Acknowledgments

This work was supported through the Office of Science of the U.S. Department of Energy (DOE) under award no. DE SC0004993 to the Joint Center for Artificial Photosynthesis, a DOE Energy Innovation Hub. The Advanced Light Source is supported by the Director, Office of Science, Office of Basic Energy Sciences, of the U.S. Department of Energy under Contract No. DE AC02 05CH11231. We thank Dr. Philip Ross for contributions to the conceptual development of the AP-XPS end station and experimental design.

References

1. H. Gerischer, *Journal of Electroanalytical Chemistry and Interfacial Electrochemistry*, **58**, 263 (1975).
2. Y. Ping, W. A. Goddard III, and G. A. Galli, *J. Am. Chem. Soc.*, **137**, 5264 (2015).
3. H. J. Lewerenz, *J. Electrochem. Soc.*, **139**, L21 (1992).
4. H. J. Lewerenz, T. Bitzer, M. Gruyters, and K. Jacobi, *J. Electrochem. Soc.*, **140**, L44 (1993).
5. K. Jacobi et al., *Phys. Rev. B*, **51**, 5437 (1995).
6. S. Axnanda et al., *Sci. Rep.*, **5**, 9788 (2015).

7. M. F. Lichterman et al., *Energ. Environ. Sci.*, **8**, 2409 (2015).
8. K. Sun et al., *Energy Environ. Sci.*, **5**, 7872 (2012).
9. K. Sun et al., *P Natl Acad Sci USA*, **112**, 3612 (2015).
10. K. Sun et al., *Phys. Chem. Chem. Phys.*, **16**, 4612 (2014).
11. Y. W. Chen et al., *Nat. Mater.*, **10**, 539 (2011).
12. S. Hu et al., *Science*, **344**, 1005 (2014).
13. M. F. Lichterman et al., *Energy Environ. Sci.*, **7**, 3334 (2014).
14. M. F. Lichterman et al., *Catal Today* (2015).
15. B. Mei et al., *J. Phys. Chem. C*, **119**, 15019 (2015).
16. P. Reckers et al., *J. Phys. Chem. C*, **119**, 9890 (2015).
17. M. T. McDowell et al., *ACS Appl. Mater. Interfaces*, **7**, 15189 (2015).
18. B. Seger et al., *J. Mater. Chem. A*, **1**, 15089 (2013).
19. Y. Lin et al., *J. Phys. Chem. C*, **119**, 2308 (2015).
20. B. Seger et al., *Rsc Adv*, **3**, 25902 (2013).
21. M. F. Lichterman et al., *ECS Transactions*, **66**, 97 (2015).
22. M. H. Richter et al., *ECS Transactions*, **66**, 105 (2015).
23. M. E. G. Lyons, R. L. Doyle, I. Godwin, M. O'Brien, and L. Russell, *J. Electrochem. Soc.*, **159**, H932 (2012).